

# Resonance Production of Excited $u$ -quark at FCC Based $\gamma p$ Colliders

YUSUF OGUZHAN GÜNAYDIN

Department of Physics, Kahramanmaraş Sutcu Imam University, Kahramanmaraş, Turkey  
MEHMET SAHIN

Department of Physics, Usak University, Usak, Turkey  
SALEH SULTANSOY

TOBB University of Economics and Technology, Ankara, Turkey  
ANAS Institute of Physics, Baku, Azerbaijan

Several Beyond the Standard Model theories are proposed that fermions might have composite substructure. The existence of excited quarks is going to be the noticeable proof for the compositeness of Standard Model fermions. For this reason, excited quarks have been investigated by phenomenological and experimental high energy physicists at various collider options for the last few decades. The Future Circular Collider (FCC) has been recently planned as particle accelerator to be established at CERN. Beside the  $\sqrt{s} = 100$  TeV proton-proton collisions, the FCC includes electron-positron and electron-proton collision options. Construction of linear  $e^-e^+$  colliders (or dedicated e-linac) tangential to the FCC will afford an opportunity to handle multi-TeV  $ep$  and  $\gamma p$  collisions. In this respect, we executed a simulation of the resonance production of the excited  $u$  quark at the FCC based  $\gamma p$  colliders with choosing both the polarized and unpolarized photon beams. The findings revealed that the chirality structure of the  $q^*-q-\gamma$  vertex can be determined by the photon beam polarization. The attainable mass limits of the excited  $u$  quark reached the highest values when the polarized photon beam was chosen. In addition, the ultimate compositeness scale values can be handled by appropriate choice of the photon beam polarization.

## 1. Introduction

The Standard Model (SM), the most reliable theory in particle physics, shows incredible consistency with experiments and reaches its last prediction after the CMS and the ATLAS collaborations, which both declared the detection of the Higgs boson [1, 2] in 2012. Despite the marvelous success of the SM on a wide range of phenomena in particle physics, there remains unsolved mysteries that

the SM does not explain. The quark-lepton symmetry, family replication, charge quantization, plenty numbers of elementary particles, parameters and the like are unsolved issues in the SM frame. Therefore, numerous models are proposed in an attempt to answer the afore-mentioned problems. One of these approaches; namely, compositeness has an assumption that SM fermions are compound states of more fundamental particles; preons [3, 4]. Numerous preonic models have been suggested by particle physicists for more than forty years [5–14]. Due to preonic interactions caused by preon models, plenty of new types of particles are expected, such as excited quarks and leptons, leptoquarks, leptogluons, diquarks, color sextet quarks, dileptons and so on.

Excited fermions are comprised of excited quarks ( $q^*$ ) and leptons ( $l^*$ ) that can be considered as the excited state of SM fermions. They could have spin-1/2 and spin-3/2 states and their masses are expected much heavier than SM fermions. As a result, the discovery of excited fermions will be a direct proof of SM quarks' and leptons' compositeness. After the first publication about excited leptons which was written in 1965 [15], scores of theoretical, phenomenological [16–34] and experimental [35–47] researchers has been focused on proving the existence of excited fermions. The historical development of fundamental blocks of the matter [48] shows that new substructures of elementary particles are discovered by new experimental findings and this evidence attracts attention of particle physicists to do research on excited quarks and leptons.

Excited quarks decay into four final states with light jets of ( $q^* \rightarrow jj$ ), ( $q^* \rightarrow j\gamma$ ), ( $q^* \rightarrow jW$ ), and ( $q^* \rightarrow jZ$ ). The most recent experimental results regarding excited quark mass are provided by the CMS and ATLAS collaborations [41–47, 49].  $q^*$  mass exclusion limits are  $m_{q^*} = 6.0$  TeV for  $q^* \rightarrow jj$ ,  $m_{q^*} = 5.5$  TeV for  $q^* \rightarrow j\gamma$ ,  $m_{q^*} = 3.2$  TeV for  $q^* \rightarrow jW$  and  $m_{q^*} = 2.9$  TeV for  $q^* \rightarrow jZ$ . For these experimental limits on excited quark mass, compositeness scale ( $\Lambda$ ) is considered to be equal to  $m_{q^*}$ .

In this paper, we investigate resonant production of the up-type excited quark ( $u^*$ ) with dijet final state at two different center of mass (CM) energies [50] of the Future Circular Collider (FCC) [51] based  $\gamma p$ -colliders [52]. In addition, we neglect possible contact interactions at this stage. We present the FCC based colliders options and their parameters, specifically  $\gamma p$ -colliders in the section 2,  $q^*$  effective interaction Lagrangian and decay width in the section 3 and leading order production cross sections and signal-background analysis using unpolarized and polarized photons in the section 4. Finally, outcomes of the  $u^*$  mass limitations, the compositeness scale ( $\Lambda$ ) inquiries and interpretation of our findings are presented in the last section.

## 2. FCC based $\gamma p$ -colliders

Throughout the last 40 years of the particle accelerator development, several groups and collaborations proposed linac-ring type colliders (see reviews [53–59]). Concerning energy frontier lepton-hadron options, VLEPP+UNK, THERA and LHeC were proposed in the 1980s, 1990s and 2000s, respectively. The latter option [60] is planned to be established at CERN around the 2020s. Furthermore, after the Large Hadron Collider (LHC) physics program are completed, the FCC [61] will be seen as experimental particle physics frontier machine by the high energy physics community. The FCC is planned nearly 4 times bigger circumferences (Figure 1) and about 7 times higher center of mass energy than the LHC. The FCC is considered as three options; (1) the electron-positron (FCC-ee) [62], (2) the proton-proton (FCC-pp) [63] and (3) the electron-proton (FCC-ep) [61] colliders. To measure new findings with high precision, FCC-ee is an appropriate option, notwithstanding, FCC-pp and FCC-ep are needed for deep investigation of interactions. That is, many features of the Higgs boson can be measured by FCC-ee whose collision energy varies between 91 and 350 GeV. However, further measurements like Higgs self-interactions and top quark Higgs bosons interaction could be achieved by FCC-pp at 100 TeV center of mass energy. Besides, quark substructure discovery might be happen at the FCC-ep collider.

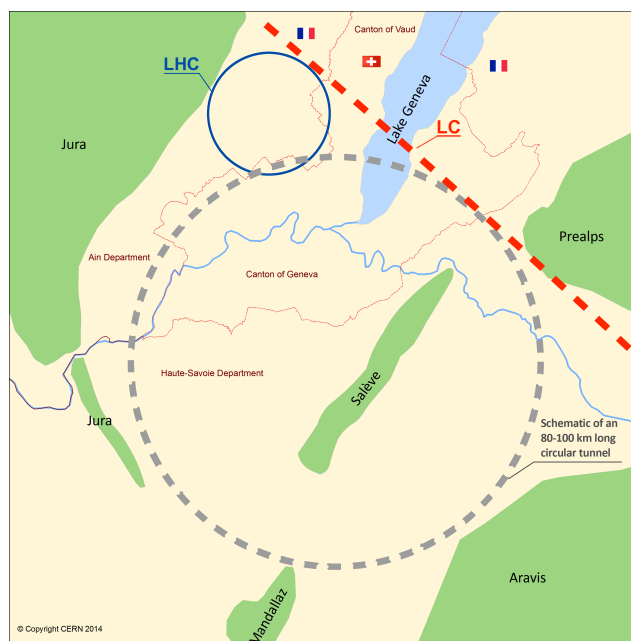


Fig. 1. Schematic drawing of the Future Circular Collider and the Linear Collider

With respect to excited quark, we focused on the FCC based  $\gamma p$  collider within

the scope of this study. There are several options for lepton-hadron collision but we preferred the FCC based electron-proton colliders by using International Linear Collider (ILC) and Plasma Wakefield Accelerator-Linear Collider (PWFA-LC) [50]. In addition to the FCC based  $ep$  colliders,  $\gamma p$  colliders [52, 64] could be utilized by exploiting Compton backscattering [65–67]. Main parameters of the  $ep$  and  $\gamma p$  colliders which we used in our calculations are listed in Table 1.

Table 1. Energy and luminosity parameters of the ILC $\otimes$ FCC and PWFA-LC $\otimes$ FCC based  $ep$  and  $\gamma p$  colliders

Collider Name	$E_e$ (TeV)	$E_\gamma^{max}$ (TeV)	$\sqrt{s_{ep}}$ (TeV)	$\sqrt{s_{\gamma p}^{max}}$ (TeV)	$\mathcal{L}_{int}$ ( $fb^{-1}/year$ )
ILC $\otimes$ FCC	0.5	0.42	10	9.1	10-100
PWFA-LC $\otimes$ FCC	5	4.15	31.6	28.8	1-10

### 3. Spin-1/2 excited quark interaction Lagrangian and decay width

Interaction between spin-1/2 excited quarks, SM quarks and gauge bosons is described by the magnetic type effective Lagrangian [17, 19, 22, 49] :

$$L_{eff} = \frac{1}{2\Lambda} \bar{q}^* \sigma^{\mu\nu} [g_s f_s \frac{\lambda^a}{2} F_{\mu\nu}^a + g f \frac{\vec{\tau}}{2} W_{\mu\nu} + g' f' \frac{Y}{2} B_{\mu\nu}] (\eta_L \frac{1-\gamma_5}{2} + \eta_R \frac{1+\gamma_5}{2}) q + H.c.. \quad (1)$$

As illustrated above,  $\Lambda$  denotes compositeness scale,  $q^*$  and  $q$  represent spin-1/2 excited quark and ground state quark respectively,  $F_{\mu\nu}^a$ ,  $W_{\mu\nu}$ ,  $B_{\mu\nu}$  are the field strength tensors for gluon, SU(2) and U(1),  $\lambda^a$  are  $3 \times 3$  Gell-Mann matrices,  $\vec{\tau}$  is the Pauli spin matrices,  $Y = 1/3$  is weak hypercharge,  $g_s$ ,  $g$ ,  $g'$  are gauge coupling constants,  $f_s$ ,  $f$  and  $f'$  are free parameters that are chosen equal to 1.  $\eta_L$  and  $\eta_R$  are the left-handed and the right-handed chirality factors, respectively. The couplings  $\eta_{L/R}$  are uniquely defined by the gauge-group representation of the excited states:  $\eta_L$  is only possible if the right-handed excited quarks are isospin doublets, while  $\eta_R$  is only possible if the left-handed excited quarks are isospin singlets. The normalization of the coupling was chosen such that  $max(|\eta_L|, |\eta_R|) = 1$  and chirality conservation requires  $\eta_L \eta_R = 0$  [49].

We implemented this interaction Lagrangian into CalcHEP software [68] by using LanHEP [69, 70]. As we earlier mention in Section 1, there are four decay channels for  $q^*$  and we plotted total decay width with respect to the excited quark mass by taking compositeness scale equals  $q^*$  mass and  $\Lambda = 30$  TeV in Figure 2. It is illustrated that excited quark mass values are correlated with decay widths positively.

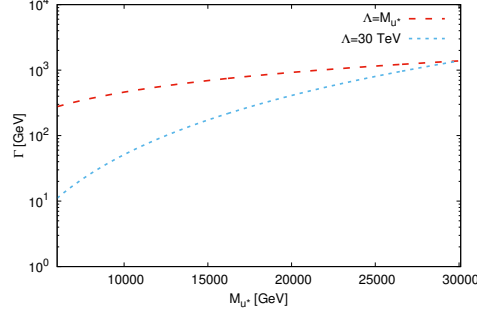


Fig. 2.  $u^*$  decay width correlations with excited quark mass at  $u^*$  mass equals compositeness scale and  $\Lambda = 30$  TeV

#### 4. Excited $u$ -quark production via proton collisions with unpolarized and polarized photon at $\sqrt{s_{\gamma p}} = 9.1$ and 28.8 TeV

In our calculation, we used two types of particle beams; proton and photon (see Section 2). 50 TeV proton beam comes from the FCC and we chose CTEQ6L quark distribution function [71, 72] with factorization and renormalization scales equal to  $M_{u^*}$  in numerical calculations. On the other hand, we had polarized and unpolarized high energy photon beams [73, 74], which were obtained from Compton backscattering [65–67] of laser beam on ILC or PWFA-LC electrons. The Feynman diagram for resonant production of  $u^*$  in photon-proton collisions is presented in Figure 3.

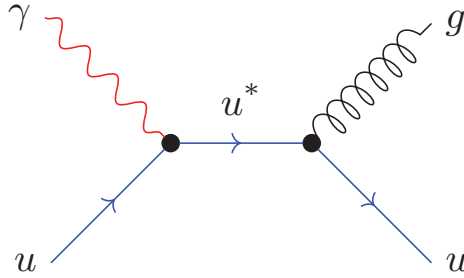


Fig. 3. Feynman diagram for signal.

##### 4.1. Cross Sections

In numerical calculations, we chose  $\eta_L = 1$ ,  $\eta_R = 0$  option for interaction Lagrangian (Eq. 1). Following, we inserted corresponding electron and proton energies and chose laser photon option which corresponds to Compton

backscattering photons in CalcHEP framework. The energy spectrum of backscattered laser photons, we used, is given in Refs. [65–67, 75] with a detailed explanation.

Figure 4 shows the cross section values with respect to  $u^*$  mass for polarized (helicity  $\gamma_H$  equals 1 and -1) and unpolarized ( $\gamma_H = 0$ ) photon beams colliding with proton beam at 9.1 TeV center of mass energy. It is seen that excited quark could be produced with sufficiently high cross section up to roughly 8 TeV both for  $\Lambda = 10$  TeV and  $\Lambda = M_{u^*}$ , corresponding to 10 events for  $100 \text{ fb}^{-1}$  luminosity value.

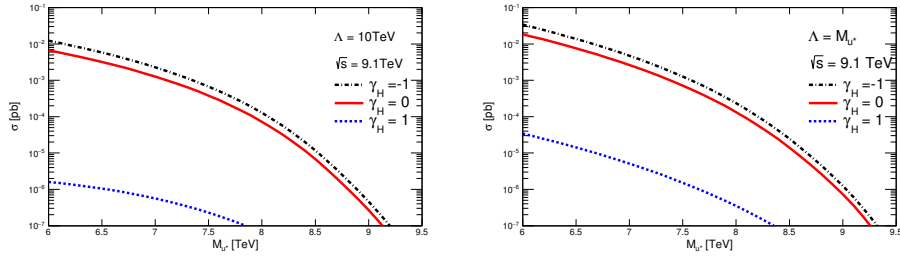


Fig. 4.  $u^*$  cross section values with respect to its mass for proton collision with both polarized and unpolarized photon beams at  $\sqrt{s} = 9.1$  TeV. On the left panel compositeness scale was chosen as 10 TeV and on the right panel  $u^*$  mass was taken the same as compositeness scale.

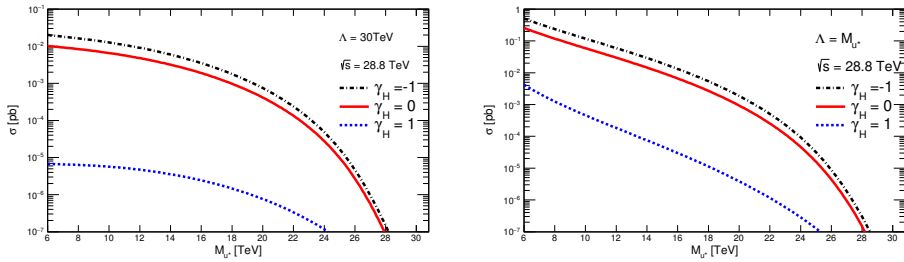


Fig. 5.  $u^*$  cross section values with respect to its mass for proton collision with both polarized and unpolarized photon beams at  $\sqrt{s} = 28.8$  TeV. On the left plot compositeness scale was chosen as 30 TeV and on the right plot  $u^*$  mass was taken the same as compositeness scale.

Figure 5 represents the same plots like the previous one but this time, the center of mass energy is 28.8 TeV. It is seen that excited quark production could be achieved at higher mass values than previous collider option due to high center of mass energy in this collider option.

## 4.2. Signal and Background Analysis

### 4.2.1. Final State Distributions and Cut Determination

Our signal process is  $\gamma + p \rightarrow u^* + X \rightarrow u + g + X$ , therefore, background processes are represented by  $\gamma + p \rightarrow j + j + X$ , where  $j$  denotes  $u, \bar{u}, d, \bar{d}, c, \bar{c}, s, \bar{s}, b, \bar{b}$  and  $g$  jets. To assign cuts for identifying the signal from background, we examined at the both signal and background transverse momentum ( $P_T$ ), the pseudo rapidity ( $\eta$ ) and the invariant mass distributions for the final state particles. Below, we present results for  $\gamma_H = -1$  case which corresponds to maximal signal cross section values. It should be noted that we normalized cross section values to plot  $P_T$  and  $\eta$  distributions for obtaining the cuts.

$P_T$  distributions of the signal are the same for the two final state particles ( $u, g$ ) and the background  $P_T$  distributions final state particles that are jets, defined above. Figure 6 demonstrates  $P_T$  distributions of the signal and the background final state jets for both two center of mass energy options. As expected for a single resonance, the usual Jacobean peaks appear for all mass values (6, 7, 10 and 15 TeV) of the signal. It is seen that when the applied  $P_T$  cut was taken 500 GeV for the  $\sqrt{s} = 9.1$  TeV and 1000 GeV for the  $\sqrt{s} = 28.8$  TeV, the background was reduced almost completely but the signal was remained nearly unchanged.

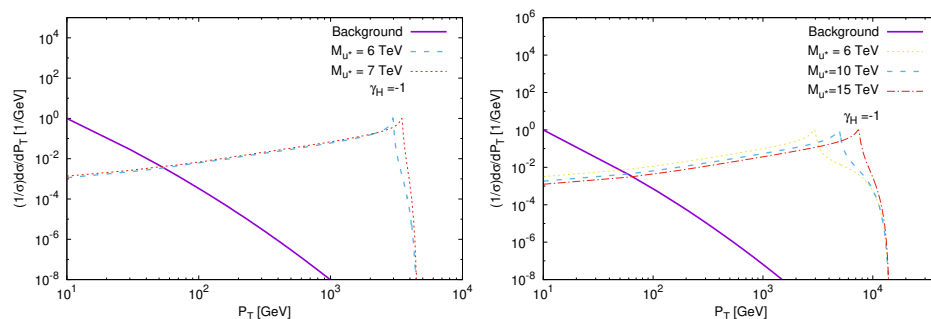


Fig. 6. Normalized  $P_T$  distributions of background and signal processes for  $\sqrt{s} = 9.1$  TeV at the left panel and for  $\sqrt{s} = 28.8$  TeV at the right panel.

When the colliding beams have different energies, asymmetry occurs in signal and background distributions. So, we extracted  $\eta$  cuts using signal and background final state jet distributions at their crossing point of their right side limits, that are shown for both center of mass energies in Figure 7.  $\eta$  distributions are presented as sum of both final state particles contributions because it is hard to identify gluon and u-quark apart. On the other hand, we applied  $\eta$  cuts as  $-5.2$  for the left hand side of the  $\eta$  distributions, this value was taken from the CMS experiment forward sub-detector limits [76]. We summarized all  $\eta$  cuts in Table 2.

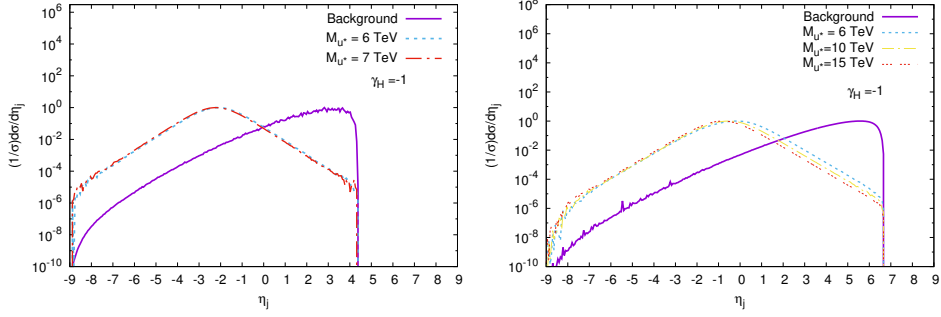


Fig. 7. Normalized  $\eta$  distributions of background and signal processes for  $\sqrt{s} = 9.1$  TeV at the left panel and for  $\sqrt{s} = 28.8$  TeV at the right panel.

Invariant mass distributions for signal and background processes are presented in Figure 8. It is seen that signal peak values are above the background, so we determined invariant mass cut as  $M_{U^*} - 2\Gamma_{U^*}$  and  $M_{U^*} + 2\Gamma_{U^*}$  mass window, where  $M_{U^*}$  is  $u^*$  mass and  $\Gamma_{U^*}$  is the decay widths of the  $u^*$ .

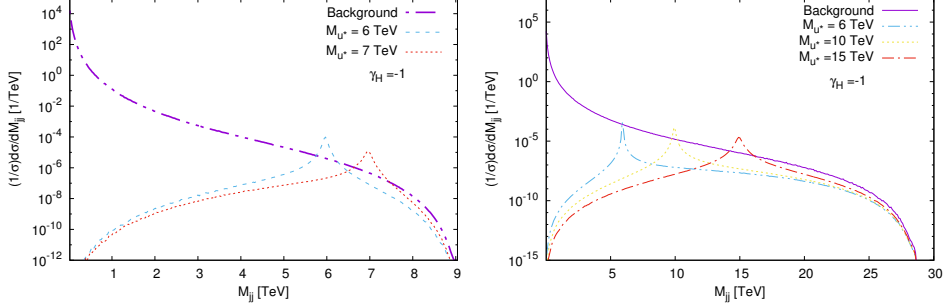


Fig. 8. Signal and background invariant mass distributions for  $\sqrt{s} = 9.1$  TeV (the left panel) and  $\sqrt{s} = 28.8$  TeV (the right panel) with  $\gamma_{\mathcal{H}} = -1$ .

Table 2. List of the pseudo rapidity cut limits for both center of mass energy options.

$\sqrt{s}$ (TeV)	9.1				28.8			
	-1		0		-1		0	
Cut Limits	Min	Max	Min	Max	Min	Max	Min	Max
$\eta_j$	-5.2	0.0	-5.2	-0.2	-5.2	2.1	-5.2	2.0



#### 4.2.2. Mass Limits Dependence on Integrated Luminosity and Photon Beam Polarization

To extract the signal from the background, we used the cuts that were determined by distribution plots in the previous subsection. After that, Equation 2 was utilized to calculate the statistical significance,

$$S = \frac{\sigma_s}{\sqrt{\sigma_s + \sigma_B}} \sqrt{\mathcal{L}_{int}} \quad (2)$$

where,  $\sigma_s$  and  $\sigma_B$  are the signal and background cross section values, respectively and  $\mathcal{L}_{int}$  is the integrated luminosity. Obtained  $u^*$  mass limits were listed in Tables 3 and 4 for both center of mass energies 9.1 TeV and 28.8 TeV colliders, respectively. According to Table 1, integrated luminosity values are 10-100  $fb^{-1}$  for ILC $\otimes$ FCC and 1-10  $fb^{-1}$  for PWFA-LC $\otimes$ FCC options. As expected, higher integrated luminosity increased mass limits for  $u^*$ . Besides, it can be seen from Tables 3 and 4 that photon beam polarization enhanced  $u^*$  mass limits 0.21 TeV for 9.1 TeV CM and approximately 1.5 TeV for 28.8 TeV CM at their upper luminosity values if compared to unpolarized photon beam-proton collisions. In addition, the attainable best  $u^*$  mass limits could be achieved when the  $\Lambda = M_{u^*}$ .

Table 3. Excited u quark mass limits for 9.1 TeV center of mass energy  $\gamma p$  collider.

$\sqrt{s}$		9.1 TeV							
$\mathcal{L}_{int}$		10 $fb^{-1}$				100 $fb^{-1}$			
$\Lambda$		10 TeV		$M_{u^*}$		10 TeV		$M_{u^*}$	
$\gamma_{\mathcal{H}}$		-1	0	-1	0	-1	0	-1	0
Mass Limits (TeV)	$5\sigma$	6.97	6.58	7.27	6.96	7.82	7.60	7.99	7.78
	$3\sigma$	7.41	7.11	7.62	7.37	8.08	7.90	8.23	8.05
	$2\sigma$	7.68	7.43	7.86	7.64	8.24	8.10	8.40	8.24

Table 4. Excited u quark mass limits for 28.8 TeV center of mass energy  $\gamma p$  collider.

$\sqrt{s}$		28.8 TeV							
$\mathcal{L}_{int}$		1 $fb^{-1}$				10 $fb^{-1}$			
$\Lambda$		15 TeV		$M_{u^*}$		30 TeV		$M_{u^*}$	
$\gamma_{\mathcal{H}}$		-1	0	-1	0	-1	0	-1	0
Mass Limits (TeV)	$5\sigma$	13.8	8.94	14.2	12.1	17.1	14.5	19.4	17.9
	$3\sigma$	17.4	14.9	16.8	14.9	19.7	17.9	21.1	19.9
	$2\sigma$	19.5	17.6	18.5	16.9	21.3	19.8	22.2	21.2

In Figure 9, we scanned luminosity values needed for the discovery ( $5\sigma$ ), observation ( $3\sigma$ ) and exclusion ( $2\sigma$ ) of  $u^*$  as a function of its mass. It is seen that photon beam polarization enhanced attainable mass limits of  $u^*$ .

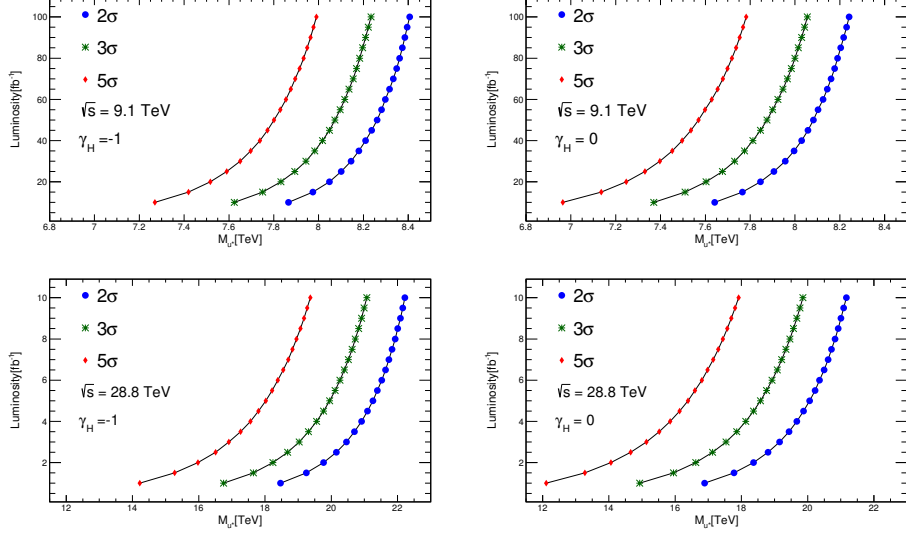


Fig. 9. The first row represents luminosity and  $u^*$  mass relations for  $\sqrt{s} = 9.1$  TeV and the second row shows the same relations for  $\sqrt{s} = 28.8$  TeV with  $\Lambda = M_{u^*}$  at three different significance values. The left column corresponds to  $\gamma_H = -1$  and the right panel corresponds to  $\gamma_H = 0$ .

#### 4.2.3. Attainable Compositeness Scale

We took compositeness scale equals  $u^*$  mass or some specific values as 10, 15 and 30 TeV until this subsection. At this point, we scanned both the compositeness scale values and  $u^*$  mass for discovery ( $5\sigma$ ), observation ( $3\sigma$ ) and exclusion ( $2\sigma$ ) mass limits. It can be clearly noticed from Figures 10 and 11 that the higher compositeness scales correspond to the lower  $u^*$  mass values. As it was expected, when the center of mass energy reached the 28.8 TeV with the highest luminosity value, the compositeness scale values had risen to the highest level for all  $u^*$  mass spectra. Furthermore, the photon beam polarization will afford an opportunity to probe bigger compositeness scale values than the unpolarized photon beam-proton collision.

In Tables 5 and 6, we summarize the highest attainable compositeness scale quantities for various  $M_{u^*}$  values at the highest integrated luminosity values for both  $\gamma p$  collider options. It is clearly seen that when the photon beam polarization is in charge, compositeness scale values increase for the whole  $M_{u^*}$  values. To illustrate, when we checked the compositeness scale values for  $\sqrt{s} = 9.1$  TeV collider option with  $M_{u^*} = 6$  TeV, the  $\Lambda$  value increased to 70.5 TeV from 48.7 TeV at the  $5\sigma$  significance. Similarly, the compositeness scale value rose to 77.9 TeV from 51.9 TeV for  $\sqrt{s} = 28.8$  TeV collider option with the same  $u^*$  mass

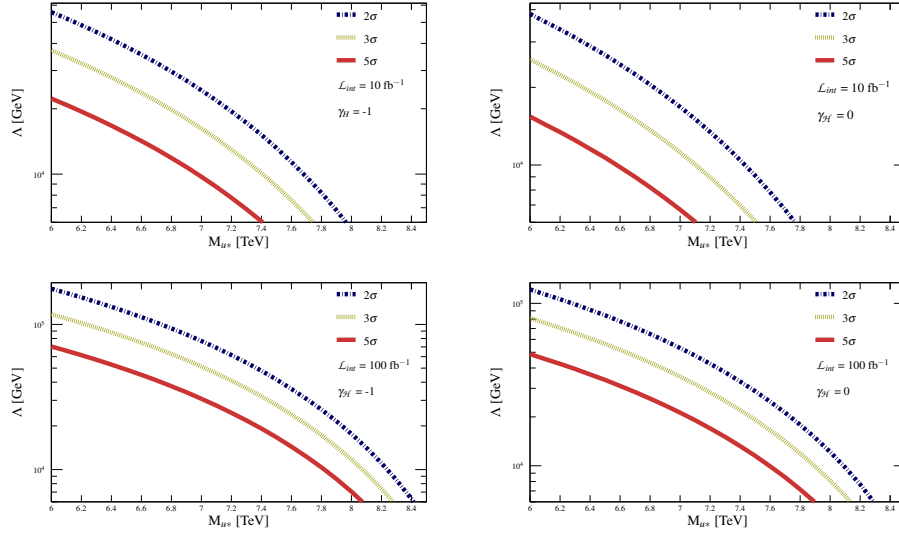


Fig. 10. The first row represents attainable  $\Lambda$  dependence on  $M_{u^*}$  for  $\mathcal{L}_{int} = 10 fb^{-1}$  and  $\sqrt{s} = 9.1$  TeV. The second row shows the same relations for the same center of mass energy and  $\mathcal{L}_{int} = 100 fb^{-1}$ .

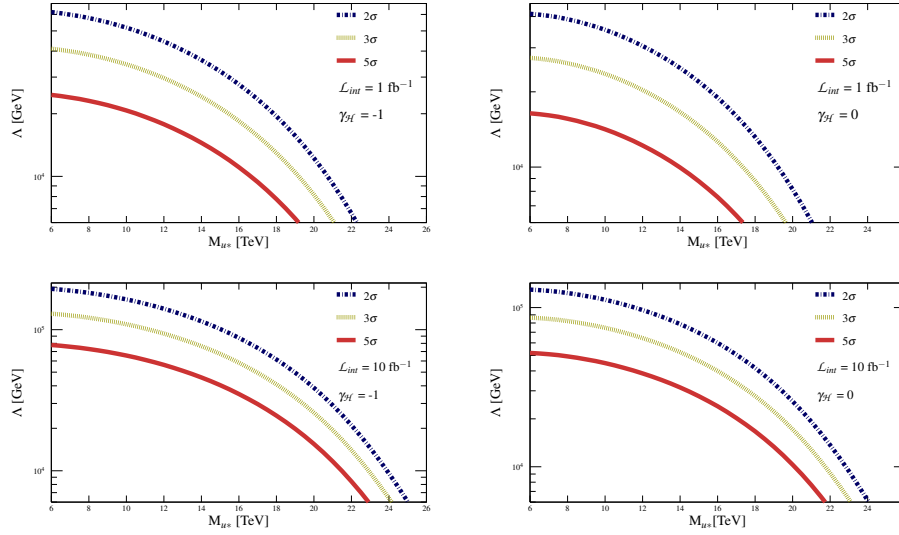


Fig. 11. The first row represents attainable  $\Lambda$  dependence on  $M_{u^*}$  for  $\mathcal{L}_{int} = 1 fb^{-1}$  and  $\sqrt{s} = 28.8$  TeV. The second row shows the same relations for the same center of mass energy and  $\mathcal{L}_{int} = 10 fb^{-1}$ .

values at the  $5\sigma$  significance.

Table 5. Attainable top  $\Lambda$  limits for  $M_{u^*}$  with the  $\mathcal{L}_{int} = 100 \text{ fb}^{-1}$ .

CM (TeV)		9.1			
$\gamma_{\mathcal{H}}$		-1		0	
$M_{u^*}$ (TeV)		6	7	6	7
$\Lambda$ (TeV)	$5\sigma$	70.5	30.8	48.7	21.2
	$3\sigma$	117	51.3	81.2	35.4
	$2\sigma$	176	76.9	122	53.1

Table 6. Attainable top  $\Lambda$  limits for  $M_{u^*}$  with the  $\mathcal{L}_{int} = 10 \text{ fb}^{-1}$ .

CM (TeV)		28.8					
$\gamma_{\mathcal{H}}$		-1			0		
$M_{u^*}$ (TeV)		6	10	15	6	10	15
$\Lambda$ (TeV)	$5\sigma$	77.9	65.6	40.5	51.9	44.8	27.7
	$3\sigma$	130	109	67.4	86.5	74.7	46.2
	$2\sigma$	195	164	101	130	112	69.4

#### 4.2.4. Determination of the Chirality Structure of the $q^*-q-\gamma$ Vertex

The FCC-pp collider option will afford an opportunity to investigate  $M_{u^*}$  up to 50 TeV mass limit [77] which essentially exceeds potential capacity of  $\gamma p$  collider options. However, the  $q^*-q-\gamma$  vertex could not be determined because the proton beams are unpolarized. The FCC based  $\gamma p$  colliders have capability to handle polarized photon beam which will allow to determine chirality structure of the excited quark interactions. Afterward, we executed asymmetry calculations taking compositeness scales equal  $u^*$  mass for  $\eta_L = 1, \eta_R = 0$  and  $\eta_L = 0, \eta_R = 1$  choices ( $\eta_L$  and  $\eta_R$  are chirality factors in Equation 1). Chirality structure of the  $q^*-q-\gamma$  vertex are distinguished by looking at the asymmetry numbers given in Table 7. Asymmetry calculation is done by Equation 3:

$$\mathcal{A} = \frac{\sigma(\gamma_{\mathcal{H}} = 1) - \sigma(\gamma_{\mathcal{H}} = -1)}{\sigma(\gamma_{\mathcal{H}} = 1) + \sigma(\gamma_{\mathcal{H}} = -1)} \quad (3)$$

where  $\mathcal{A}$  denotes asymmetry,  $\sigma(\gamma_{\mathcal{H}} = -1)$  corresponds to the cross section numbers with helicity equal to -1 and  $\sigma(\gamma_{\mathcal{H}} = 1)$  represents to cross section numbers with helicity equal to 1.

## 5. Conclusion

In this work, we analyzed resonance production of the excited  $u$  quark at the FCC based  $\gamma p$  colliders that offer two possibilities:  $\sqrt{s}_{\gamma p}^{max} = 9.1 \text{ TeV}$  with  $\mathcal{L}_{int} =$

Table 7. The polarization asymmetry for the excited  $u$  quark

CM (TeV)	$M_{u^*}$ (TeV)	$\gamma_{\mathcal{H}}$	$\eta_L = 1, \eta_R = 0$		$\eta_L = 0, \eta_R = 1$	
			$\sigma$ (pb)	$\mathcal{A}$	$\sigma$ (pb)	$\mathcal{A}$
9.1	6	-1	$4.15 \times 10^{-2}$	-0.99	$8.07 \times 10^{-5}$	0.99
		1	$1.71 \times 10^{-4}$		$2.29 \times 10^{-2}$	
	7	-1	$6.50 \times 10^{-3}$	-0.98	$2.78 \times 10^{-5}$	0.98
		1	$5.89 \times 10^{-5}$		$3.54 \times 10^{-3}$	
28.8	10	-1	$1.39 \times 10^{-1}$	-0.99	$4.34 \times 10^{-4}$	0.99
		1	$9.20 \times 10^{-4}$		$7.61 \times 10^{-2}$	
	15	-1	$2.23 \times 10^{-2}$	-0.99	$3.56 \times 10^{-5}$	0.99
		1	$7.54 \times 10^{-5}$		$1.23 \times 10^{-2}$	

10-100  $fb^{-1}$  (ILC $\otimes$ FCC) and  $\sqrt{s}_{\gamma p}^{max} = 28.8$  TeV with  $\mathcal{L}_{int} = 1-10$   $fb^{-1}$  (PWFA-LC $\otimes$ FCC). It should be noted that at this stage, we did not consider hadronization and detector effects which may lead to some decrease of discovery limits on  $u^*$  mass and compositeness scale.

We conducted calculation of the  $u^*$  mass limits for discovery ( $5\sigma$ ), observation ( $3\sigma$ ) and exclusion ( $2\sigma$ ) confidence levels at the 10, 15, 30 TeV compositeness scales and at  $\Lambda = M_{u^*}$ , but the highest mass limits are achieved by taking  $M_{u^*}$  equals  $\Lambda$ . As seen from Tables 3 and 4, the photon beam polarization increases the mass limits for all confidence levels. For  $\gamma_{\mathcal{H}} = -1$ ,  $\Lambda = M_{u^*}$  and  $\mathcal{L}_{int} = 100$   $fb^{-1}$ , attainable mass limits are 7.99 TeV for  $5\sigma$ , 8.23 TeV for  $3\sigma$  and 8.40 TeV for  $2\sigma$  at  $\sqrt{s} = 9.1$  TeV collider option. Concerning the highest center of mass energy collider option ( $\sqrt{s} = 28.8$  TeV), the biggest attainable mass limits become 19.4 TeV for  $5\sigma$ , 21.1 TeV for  $3\sigma$  and 22.2 TeV for  $2\sigma$  confidence levels. To address these findings, ATLAS and CMS excluded  $M_{u^*}$  up to 6 TeV with 37  $fb^{-1}$  integrated luminosity at  $\sqrt{s} = 13$  TeV (with  $\sqrt{s} = 14$  TeV and  $\mathcal{L}_{int} = 300$   $fb^{-1}$  this limit will potentially increase to  $M_{u^*} = 7.5$  TeV). Therefore, the FCC- $\gamma p$  collider essentially superiors (3 times) the LHC potential.

Besides the specific values of the compositeness scale, we scanned the compositeness scale with respect to  $M_{u^*}$ . Our calculation results show that the highest compositeness scale value is provided by the photon beam polarization (see Tables 5 and 6). Compositeness scale values are evaluated as 77.9 TeV for  $5\sigma$ , 130 TeV for  $3\sigma$  and 195 TeV for  $2\sigma$  at the  $\sqrt{s} = 28.8$  TeV with  $\mathcal{L}_{int} = 10$   $fb^{-1}$ ,  $M_{u^*} = 6$  TeV and  $\gamma_{\mathcal{H}} = -1$ . These values essentially exceed the LHC potential but the FCC-pp is much higher [77].

Finally, if the excited quarks mass lies in the region mentioned above, the FCC-pp collider will apparently discover  $u^*$  before the construction of FCC based  $\gamma p$  colliders. However, as seen from this study, latter ones will provide unique opportunity to determine chirality structure of  $u^*-u-\gamma$  vertex by using the polarized

photon beam.

## 6. Acknowledgements

This study is supported by TUBITAK under the grant No: 114F337. We thank Professor Yasar Onel for his support and contribution for encouraging such a research.

## REFERENCES

- [1] S. Chatrchyan et al. Observation of a new boson at a mass of 125 GeV with the CMS experiment at the LHC. *Physics Letters B*, 716(1):30 – 61, 2012.
- [2] G. Aad et al. Observation of a new particle in the search for the Standard Model Higgs boson with the ATLAS detector at the LHC. *Physics Letters B*, 716(1):1 – 29, 2012.
- [3] J. C. Pati and A. Salam. Lepton number as the fourth "color". *Physical Review D*, 10(1):275–289, 1974. Erratum *ibid.* 11, 703 (1975).
- [4] I. A. D'Souza and C. S. Kalman. *Preons: Models of leptons, quarks and gauge bosons as composite objects*. World Scientific, 1992.
- [5] M.A. Shupe. A composite model of leptons and quarks. *Physics Letters B*, 86:87–92, 1979.
- [6] H. Harari. A schematic model of quarks and leptons. *Physics Letters B*, 86(1):83–86, 1979.
- [7] H. Terazawa. Subquark model of leptons and quarks. *Physical Review D*, 22(1):184, 1980.
- [8] H. Terazawa, M. Yasuè, K. Akama, and M. Hayashi. Observable effects of the possible sub-structure of leptons and quarks. *Physics Letters B*, 112(4):387 – 392, 1982.
- [9] H. Terazawa. A fundamental theory of composite particles and fields. *Physics Letters B*, 133(1):57 – 60, 1983.
- [10] E. J. Eichten, K. D. Lane, and M. E. Peskin. New tests for quark and lepton substructure. *Physical Review Letters*, 50(11):811–814, 1983.
- [11] H. Fritzsch and G. Mandelbaum. Weak interactions as manifestations of the substructure of leptons and quarks. *Physics Letters B*, 102(5):319 – 322, 1981.

- [12] A. Çelikel, M. Kantar, and S. Sultansoy. A search for sextet quarks and leptogluons at the lhc. *Physics Letters B*, 443(1):359 – 364, 1998.
- [13] M.E. De Souza. Weak decays of hadrons reveal compositeness of quarks. *Scientia Plena*, 4(6), 2008.
- [14] H. Fritzsch. Composite Weak Bosons at the Large Hadronic Collider. *Mod. Phys. Lett.*, A31(20):1630019, 2016.
- [15] F. E. Low. Heavy electrons and muons. *Phys. Rev. Lett.*, 14:238–239, Feb 1965.
- [16] F.M. Renard. Excited quarks and new hadronic states. *II Nuovo Cimento A (1971-1996)*, 77(1):1–20, 1983.
- [17] J. Kühn and P. Zerwas. Excited quarks and leptons. *Physics Letters B*, 147(1-3):189–196, 1984.
- [18] G. Pancheri and Y.N. Srivastava. Weak isospin spectroscopy of excited quarks and leptons. *Physics Letters B*, 146(1-2):87–94, 1984.
- [19] A. De Rújula, L. Maiani, and R. Petronzio. Search for excited quarks. *Physics Letters B*, 140(3-4):253–258, 1984.
- [20] K. Hagiwara, S. Komamiya, and D. Zeppenfeld. Excited lepton production at LEP and HERA. *Zeitschrift für Physik C Particles and Fields*, 29(1):115–122, 1985.
- [21] J.H. Kühn, H.D. Tholl, and P.M. Zerwas. Signals of excited quarks and leptons. *Physics Letters B*, 158(3):270–275, 1985.
- [22] U. Baur, I. Hinchliffe, and D. Zeppenfeld. Excited quark production at hadron colliders. *International Journal of Modern Physics A*, 2(04):1285–1297, 1987.
- [23] M. Spira and P.M. Zerwas. Excited quarks and leptons. In *Heavy Flavours and High-Energy Collisions in the 1–100 TeV Range*, pages 519–529. Springer, 1989.
- [24] U. Baur, M. Spira, and P.M. Zerwas. Excited-quark and-lepton production at hadron colliders. *Physical Review D*, 42(3):815, 1990.
- [25] F. Boudjema, A. Djouadi, and J. L. Kneur. Excited fermions at  $e^+e^-$  and ep colliders. *Zeitschrift für Physik C Particles and Fields*, 57(3):425–449, 1993.
- [26] O. Çakır and R. Mehdiyev. Excited quark production at the CERN LHC. *Phys. Rev. D*, 60:034004, Jun 1999.

- [27] O. Çakır, C. Leroy, and R. Mehdiyev. Search for excited quarks with the ATLAS experiment at the CERN LHC: Double jets channel. *Phys. Rev. D*, 62:114018, Nov 2000.
- [28] O. Çakır, C. Leroy, and R. Mehdiyev. Search for excited quarks with the ATLAS experiment at the CERN LHC: W/Z+jet channel. *Phys. Rev. D*, 63:094014, Apr 2001.
- [29] O. J. P. Éboli, S. M. Lietti, and P. Mathews. Excited leptons at the cern large hadron collider. *Phys. Rev. D*, 65:075003, Mar 2002.
- [30] O. Çakır, A. Yılmaz, and S. Sultansoy. Single production of excited electrons at future  $e^+e^-$ ,  $ep$  and  $pp$  colliders. *Physical Review D*, 70(7):075011, 2004.
- [31] O. Çakır, C. Leroy, R. Mehdiyev, and A. Belyaev. Production and decay of excited electrons at the LHC. *The European Physical Journal C-Particles and Fields*, 32:s1–s17, 2004.
- [32] O. Çakır and A. Ozansoy. Search for excited spin-3/2 and spin-1/2 leptons at linear colliders. *Physical Review D*, 77(3):035002, 2008.
- [33] A. Caliskan, S. O. Kara, and A. Ozansoy. Excited muon searches at the FCC based muon-hadron colliders. *Advances in High Energy Physics*, 2017:1540243, 2017.
- [34] A. Caliskan. Excited neutrino search potential of the FCC-based electron-hadron colliders. *Advances in High Energy Physics*, 2017:4726050, 2017.
- [35] F. Abe et al. Search for new particles decaying to dijets in  $p\bar{p}$  collisions at  $\sqrt{s} = 1.8$  TeV. *Phys. Rev. Lett.*, 74:3538–3543, May 1995.
- [36] C. Adloff et al. A search for excited fermions at hera. *The European Physical Journal C - Particles and Fields*, 17(4):567–581, 2000.
- [37] M. Acciarri et al. Search for excited leptons in  $e^+e^-$  interactions at  $\sqrt{s}=192$ –202 GeV. *Physics Letters B*, 502(1 - 4):37 – 50, 2001.
- [38] S. Chekanov et al. Searches for excited fermions in ep collisions at HERA. *Physics Letters B*, 549(1):32–47, 2002.
- [39] J. Abdallah et al. Search for excited leptons in  $e^+e^-$  collisions at  $\sqrt{s} = 189$ –209 GeV. *The European Physical Journal C - Particles and Fields*, 46(2):277, 2006.
- [40] V. Khachatryan et al. Search for excited quarks in the  $\gamma +$  jet final state in proton-proton collisions at  $\sqrt{s} = 8$  TeV. *Physics Letters B*, 738:274 – 293, 2014.



- [41] G. Aad et al. Search for new phenomena with photon+jet events in proton-proton collisions at  $\sqrt{s}=13$  TeV with the ATLAS detector. *Journal of High Energy Physics*, 2016(3):41, 2016.
- [42] G. Aad et al. Search for new phenomena in dijet mass and angular distributions from pp collisions at with the {ATLAS} detector. *Physics Letters B*, 754:302 – 322, 2016.
- [43] M. Aaboud et al. Search for new phenomena in dijet events using  $37 \text{ fb}^{-1}$  of  $pp$  collision data collected at  $\sqrt{s} = 13$  TeV with the ATLAS detector. Technical report, 2017.
- [44] V. Khachatryan et al. Search for narrow resonances decaying to dijets in proton-proton collisions at  $\sqrt{s}=13$  TeV. *Phys. Rev. Lett.*, 116:071801, Feb 2016.
- [45] CMS Authors. Search for excited quarks in the photon + jet final state in proton-proton collisions at  $\sqrt{s} = 13$  TeV. Technical Report CMS-PAS-EXO-16-015, CERN, Geneva, 2016.
- [46] A.M. Sirunyan et al. Search for dijet resonances in proton proton collisions at and constraints on dark matter and other models. *Physics Letters B*, 769:520 – 542, 2017.
- [47] CMS Authors. Search for excited states of light and heavy flavor quarks in the  $\gamma$ +jet final state in proton-proton collisions at  $\sqrt{s} = 13$  TeV. Technical Report CMS-PAS-EXO-17-002, CERN, Geneva, 2017.
- [48] M. Sahin, S. Sultansoy, and S. Turkoz. Search for the fourth standard model family. *Phys. Rev. D*, 83:054022, Mar 2011.
- [49] C. Patrignani et al. Review of Particle Physics. *Chin. Phys.*, C40(10):100001, 2016.
- [50] Y. C. Acar, A. N. Akay, S. Beser, A. C. Canbay, H. Karadeniz, U. Kaya, B. B. Oner, and S. Sultansoy. Future circular collider based lepton–hadron and photon–hadron colliders: Luminosity and physics. *Nuclear Instruments and Methods in Physics Research Section A: Accelerators, Spectrometers, Detectors and Associated Equipment*, 871:47 – 53, 2017.
- [51] Future Circular Collider Study Kickoff Meeting. University of Geneva, February 2014.
- [52] A.K. Çiftçi, S. Sultansoy, Ş. Türköz, and Ö. Yavaş. Main parameters of tev energy  $\gamma p$  colliders. *Nuclear Instruments and Methods in Physics Research Section A: Accelerators, Spectrometers, Detectors and Associated Equipment*, 365(2):317 – 328, 1995.

- [53] S. Sultanov. Prospects of the future  $ep$  and  $\gamma p$  colliders: Luminosity and physics. Technical report, International Centre for Theoretical Physics, 1989.
- [54] B. H. Wiik. Recent development in accelerators. *Proceedings of the Int. Europhysics Conf. on High Energy Physics (Marseille, France)*, pages 739–758, July 1993.
- [55] R. Brinkmann, A.K. Ciftci, S. Sultansoy, S. Turkoz, F. Willeke, O. Yavas, and M. Yilmaz. Linac-ring type colliders: Fourth way to tev scale. *DESY-97-239; arXiv preprint physics/9712023*, 1997.
- [56] S. Sultansoy. Four ways to tev scale; Invited talk at the International Workshop on Linac-Ring Type  $ep$  and  $\gamma p$  Colliders, Ankara, 9-11 April 1997. *Turkish Journal of Physics*, 22(7):575–594, 1998.
- [57] S. Sultansoy. The PostHERA era: Brief review of future lepton hadron and photon hadron colliders. *DESY-99-159, AU-HEP-99-02*, 1999.
- [58] S. Sultansoy. Linac-ring type colliders: Second way to tev scale. *The European Physical Journal C-Particles and Fields*, 33:s1064–s1066, 2004.
- [59] A. N. Akay, H. Karadeniz, and S. Sultansoy. Review of linac–ring-type collider proposals. *International Journal of Modern Physics A*, 25(24):4589–4602, 2010.
- [60] J. L. Abelleira Fernandez et al. A Large Hadron Electron Collider at CERN: Report on the Physics and Design Concepts for Machine and Detector. *Journal of Physics G: Nuclear and Particle Physics*, G39:075001, 2012.
- [61] M. Benedikt and F. Zimmermann. Future circular colliders. Technical report, FCC-DRAFT-ACC-2015-032, 2015.
- [62] J. Wenninger, M. Benedikt, K. Oide, and F. Zimmermann. Future circular collider study lepton collider parameters. *CERN EDMS no*, 1346082, 2014.
- [63] J. Wenninger, M. Benedikt, A. Blondel, M. Koratzinos, P. Janot, E. Jensen, B. Holzer, R. Tomas, and F. Zimmermann. Future circular collider study hadron collider parameters. Technical Report FCC-1401201640-DSC, 2014.
- [64] H. Aksakal, A.K. Ciftci, Z. Nergiz, D. Schulte, and F. Zimmermann. Conversion efficiency and luminosity for gamma-proton colliders based on the LHC-CLIC or LHC-ILC QCD explorer scheme. *Nuclear Instruments and Methods in Physics Research Section A: Accelerators, Spectrometers, Detectors and Associated Equipment*, 576(2):287 – 293, 2007.

- [65] I. F. Ginzburg, G. L. Kotkin, V. G. Serbo, and V. I. Telnov. Colliding  $ge$  and  $gg$  beams based on the single-pass  $e^+e^-$  colliders (VLEPP type). *Nuclear Instruments and Methods in Physics Research*, 205(1):47 – 68, 1983.
- [66] I.F. Ginzburg, G.L. Kotkin, S.L. Panfil, V.G. Serbo, and V.I. Telnov. Colliding  $\gamma e$  and  $\gamma\gamma$  beams based on single-pass  $e^+e^-$  accelerators II. Polarization effects, monochromatization improvement. *Nuclear Instruments and Methods in Physics Research*, 219(1):5 – 24, 1984.
- [67] V.I. Telnov. Problems in obtaining  $\gamma\gamma$  and  $\gamma e$  colliding beams at linear colliders. *Nuclear Instruments and Methods in Physics Research Section A: Accelerators, Spectrometers, Detectors and Associated Equipment*, 294(1):72 – 92, 1990.
- [68] A. Belyaev, N.D. Christensen, and A. Pukhov. CalcHEP 3.4 for collider physics within and beyond the Standard Model. *Comput. Phys. Commun.*, 184:1729–1769, 2013.
- [69] A. V. Semenov. *LanHEP: A Package for automatic generation of Feynman rules in field theory. Version 2.0*, 2002.
- [70] A. Semenov. LanHEP — A package for automatic generation of Feynman rules from the Lagrangian. Version 3.2. *Comput. Phys. Commun.*, 201:167–170, 2016.
- [71] J. Pumplin, D. R. Stump, J. Huston, H.L. Lai, P. Nadolsky, and W.K. Tung. New generation of parton distributions with uncertainties from global qcd analysis. *Journal of High Energy Physics*, 2002(07):012, 2002.
- [72] D. Stump, J. Huston, J. Pumplin, W.K. Tung, H.L. Lai, S. Kuhlmann, and J.F. Owens. Inclusive jet production, parton distributions, and the search for new physics. *Journal of High Energy Physics*, 2003(10):046, 2003.
- [73] D.L. Borden, D.A. Bauer, and D.O. Caldwell. Higgs boson production at a photon linear collider. *Phys. Rev. D*, 48:4018–4028, Nov 1993.
- [74] A. D’Angelo, O. Bartalini, V. Bellini, P.L. Sandri, D. Moricciani, L. Nicoletti, and A. Zucchiatti. Generation of compton backscattering  $\gamma$ -ray beams. *Nuclear Instruments and Methods in Physics Research Section A: Accelerators, Spectrometers, Detectors and Associated Equipment*, 455(1):1 – 6, 2000.
- [75] A. Pukhov, A. Belyaev, and N. Christensen. *CalcHEP-Calculator for High Energy Physics-a package for evaluation of Feynman diagrams, integration over multi-particle phase space, and event generation.*, CalcHEP Manual 3.3.6 edition, July 2012.

- [76] V. Khachatryan et al. Evidence for transverse-momentum-and pseudorapidity-dependent event-plane fluctuations in  $PbPb$  and  $pPb$  collisions. *Physical Review C*, 92(3):034911, 2015.
- [77] A. N. Akay, Y. O. Günaydin, M. Sahin, and S. Sultansoy. In preparation.